AD-A115 378 IBM RESEARCH LAB SAN JOSE CA F/G 7/5
THE USE OF HOLOGRAPHY TO INVESTIGATE COMPLEX PHOTOCHEMICAL REAC--ETC(U)
OCT 81 D M BURLAND, C BRAUCHLE N00014-81-C-0418
UNCLASSIFIED TR-1 NL

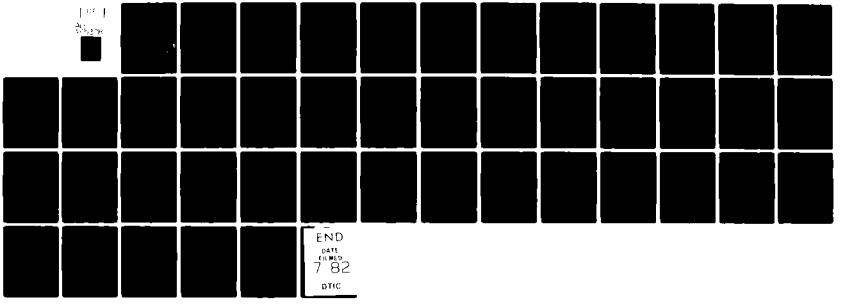

END
DATE FILMED
7 82
DTIC

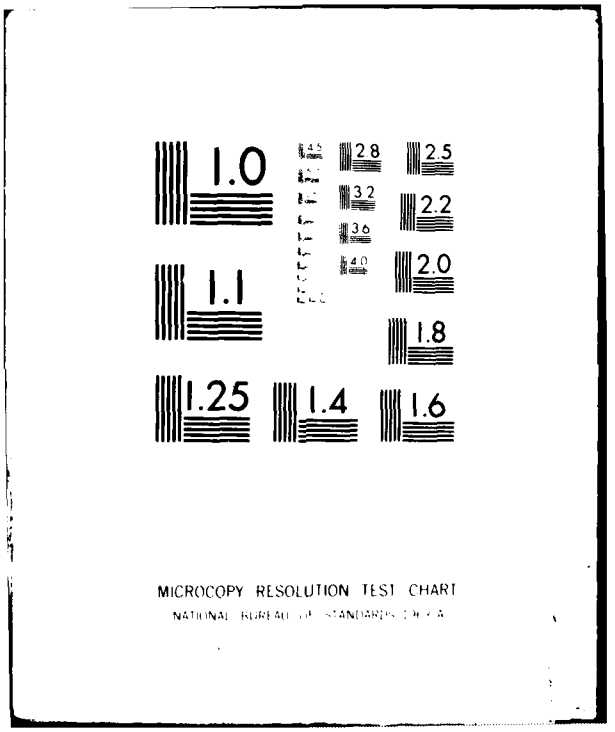
1.0
1.1
1.25
1.4
1.6
1.8
2.0
2.2
2.5
2.8
3.2
3.6
4.0
MICROCOPY RESOLUTION TEST CHART

(12)

Unclassified

SECURITY CLASSIFICATION OF THIS PAGE (When Data Entered)

REPORT DOCUMENTATION PAGE		READ INSTRUCTIONS BEFORE COMPLETING FORM
1. REPORT NUMBER: 1	2. GOVT ACCESSION NO.: AD-A115378	3. RECIPIENT'S CATALOG NUMBER
4. TITLE (and Subtitle): THE USE OF HOLOGRAPHY TO INVESTIGATE COMPLEX PHOTOCHEMICAL REACTIONS		5. TYPE OF REPORT & PERIOD COVERED: Technical Report
		6. PERFORMING ORG. REPORT NUMBER
7. AUTHOR(s): D. M. Burland and Chr. Bräuchle		8. CONTRACT OR GRANT NUMBER(s): N00014-81-C-0418
9. PERFORMING ORGANIZATION NAME AND ADDRESS: International Business Machines Corporation, San Jose Research Laboratory, 5600 Cottle Rd., San Jose, CA 95193		10. PROGRAM ELEMENT, PROJECT, TASK AREA & WORK UNIT NUMBERS: 051-782
11. CONTROLLING OFFICE NAME AND ADDRESS: Office of Naval Research Code 413, 800 N. Quincy Street, Arlington, VA 22217		12. REPORT DATE: October 13, 1981 13. NUMBER OF PAGES: 40
14. MONITORING AGENCY NAME & ADDRESS (if different from Controlling Office)		15. SECURITY CLASS. (of this report): Unclassified 15a. DECLASSIFICATION/DOWNGRADING SCHEDULE

16. DISTRIBUTION STATEMENT (of this Report)

This document has been approved for public release and sale; its distribution is unlimited

17. DISTRIBUTION STATEMENT (of the abstract entered in Block 20, if different from Report)

18. SUPPLEMENTARY NOTES

To be published in Journal of Chemical Physics

19. KEY WORDS (Continue on reverse side if necessary and identify by block number)

Holography, photochemistry, benzophenone, kinetics

20. ABSTRACT (Continue on reverse side if necessary and identify by block number)

The growth of a hologram can be used to follow the temporal course of a photochemical reaction. In this paper the application of this technique to reactions involving more than one photochemical step is considered. A theoretical framework is developed by which the hologram growth curves can be predicted provided one knows the appropriate kinetic equations. Three different kinetic schemes are explicitly considered; a one-step reaction, two parallel reactions, and a two-step consecutive reaction scheme. The

DD FORM 1 JAN 73 1473 EDITION OF 1 NOV 65 IS OBSOLETE S/N 0102-LF-014-6601

Unclassified

SECURITY CLASSIFICATION OF THIS PAGE (When Data Entered)

20. Abstract (continued)

calculations are compared with experimental results obtained for the reaction of benzophenone in polymethylmethacrylate.

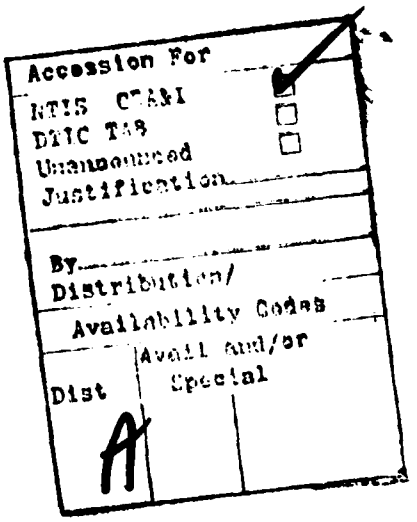

OFFICE OF NAVAL RESEARCH

Contract N00014-81-C-0418

Task No. NR 051-782

TECHNICAL REPORT NO. 1

The Use of Holography to Investigate Complex Photochemical Reactions

by

D. M. Burland and Chr. Brauchle

Prepared for Publication

in the

Journal of Chemical Physics

IBM Research Laboratory
San Jose, California 95193

October 13, 1981

I. INTRODUCTION

In previous papers we have demonstrated how the growth of a hologram in time can be used to obtain information about photochemistry [1]. In particular, we have used the technique to investigate the photochemistry of tetrazine [2], carbazole [3], and benzophenone [4], all in polymer host matrices. Traditionally the formation of holograms in polymer matrices has been of interest to those searching for new holographic materials [5]. This area has been nicely reviewed by Tomlinson and Chandross [6]. Our approach has been to turn these investigations around and to extract photochemical information from the holography.

In previous work [1b], we have developed a theory for photochemical holograms that is valid for the simple single step process where reactants go directly to products. These results are valid only for early times in the holographic growth curves. Even with these approximations we were able to obtain a considerable amount of photochemical information. The experimental work with benzophenone [4] showed, however, that in some cases it is necessary to go beyond the simple theory. The photochemistry of benzophenone is characterized by two distinct steps:

$$A \xrightarrow{n h\nu} B \xrightarrow{m h\nu} C$$

where benzophenone (A) proceeds to a product (B) that can itself undergo photochemistry yielding products (C). Here n and m are the number of photons involved in each step. For benzophenone it was found that n=m=2.

In this paper we attempt to treat the growth of a hologram in more detail with the specific example of benzophenone in mind. The approach is to introduce kinetic rate

equations [7] into the traditional equations for holographic efficiency [8]. Numerical calculations of the holographic growth curves can then be made and compared with experimentally obtained curves. A general formalism is outlined below making it possible to calculate the holographic growth curves provided one knows the kinetic equations governing the photochemical reactions. Or, turning this around, one can obtain information about the photochemical reaction scheme by comparing calculated and experimental growth curves.

II. EXPERIMENTAL DETAILS

The calculated holographic growth curves will be compared with experiments on the photochemistry of benzophenone in a polymethylmethacrylate (PMMA) matrix. Most of the details of the experimental set-up and the method of preparation of the samples have been discussed previously [1-4]. We will, therefore, only concentrate on the differences between the experiments treated here and in previous papers.

Two distinct set-ups were used to obtain the experimental results. In the arrangement shown in Figure 1, the UV lines (363.8, 351.4, 351.1, and 333.6 nm) from an Ar laser were used. The UV beam was split into two and the two beams were focused to overlapping spots about 0.004 cm^2 in area on the benzophenone/PMMA sample. The angle of interference, 2θ in the figure, was about 0.02 rad. One of the UV beams was sent through a rotating chopper wheel before it reached the sample. During the periods when this beam was off, its holographic image was produced by the other beam and monitored by a photodiode. The signal from the photodiode was sent to a boxcar integrator which 'read' the signal only when the chopper was blocking the laser beam.

The output signal from the boxcar integrator, proportional to the intensity of the hologram, was sent to both a strip chart recorder and an IBM Series/1 computer.

The second set-up was used when it was necessary to 'read' the hologram with a wavelength different from the one used to produce it. In this case a second Ar laser was used at 514.5 or 488.0 nm. The holograms were produced by the UV lines from the first laser just as indicated in Figure 1. In addition, a line from the second laser was focused onto the sample along a path nearly collinear with the unchopped beam. The two reading beams, UV and visible, were deflected by the hologram in the sample in the direction of the photodiode. A glass filter placed in front of the photodiode permitted only the visible holographic image to be detected. In this way one could follow the development of the hologram with visible light while it was being produced with interfering UV beams.

III. GENERAL THEORY OF HOLOGRAPHIC PHOTOCHEMISTRY

A. Mechanism of Hologram Production

In this section we will describe the method by which holograms are formed as a result of photochemistry in a recording medium. The relationship between the hologram efficiency and the samples optical properties has been discussed elsewhere [6] and will be only briefly discussed here. Our emphasis will be on understanding the relationship between holographic growth and the underlying photochemistry, particularly in those circumstances where the chemical reaction scheme is complex.

In Figure 2 the formation of a hologram by the interference of an object and a reference beam is shown. In the simplest case to analyze (and the case that corresponds with our experimental arrangement) the object and reference waves are plane waves.

These plane waves interfere to produce a modulated intensity pattern across the sample [1b]. The photochemical process responsible for recording the hologram depends on the light intensity at any point x across the sample. This intensity is given by

$$I = B|E_T|^2 = B\left[E_o^{obj^2} + E_o^{ref^2} + 2E_o^{obj}E_o^{ref}\cos\left(\frac{2\pi}{\Lambda}x\right)\right]$$

$$= B\left(E_o^{obj^2} + E_o^{ref^2}\right)\left\{1 + V\cos\left(\frac{2\pi}{\Lambda}x\right)\right\} \qquad (1)$$

where I is in units of einsteins/cm^2-sec and all other quantities are in cgs units. E_o^{obj} and E_o^{ref} are the electric field amplitude for object and reference waves, respectively. The proportionality constant B is given by

$$B = \frac{Ahc^2}{8\pi\lambda}\sqrt{\frac{\varepsilon}{\mu}}\,. \qquad (2)$$

Here ε and μ are the permittivity and permeability of the medium and A is Avogadro's number. Λ in Eq. (1) is the spacing between interference fringes produced by the two interfering plane waves and is given by

$$\Lambda = \frac{\lambda}{2n\sin\theta} \qquad (3)$$

V is the contrast or fringe visibility and is found to be

$$V = \frac{2E_o^{obj}E_o^{ref}}{E_o^{obj^2} + E_o^{ref^2}} = \frac{2(I^{obj}I^{ref})^{1/2}}{I^{obj} + I^{ref}}\,. \qquad (4)$$

The fringe visibility is seen to depend on the relative intensity of object (I^{obj}) and reference (I^{ref}) beams. Another way of expressing V is in terms of the maximum intensity for I

$$I_{max} = B(E_o^{obj} + E_o^{ref})^2 \tag{5}$$

and the minimum intensity

$$I_{min} = B(E_o^{obj} - E_o^{ref})^2 . \tag{6}$$

In this case

$$V = (I_{max} - I_{min})/(I_{max} + I_{min}) . \tag{7}$$

From Eq. (4) one sees that the maximum fringe visibility (V=1) is obtained when reference and object waves are of equal intensity.

Fringe visibility, as defined by Eq. (7), is degraded by other factors in addition to intensity inequalities. Motion of the holographic recording medium, relative motion of interfering object and reference beams, and frequency fluctuations in the recording beam can all cause a reduction in V [9]. As will be shown below, this can have a significant effect on the shape of the holographic growth curve.

Equation (1) expresses the variation of the total intensity across the holographic recording material. The intensity variation results at any given time in a variation of the extent of the photochemistry across the sample. This spatially nonuniform photochemistry in turn results in a spatially periodic variation in the index of refraction $n(x)$ and the absorption coefficient $a(x)$ such that:

$$n(x) = n_0 + n_1 \cos\left(\frac{2\pi}{\Lambda} x\right) + n_2 \cos\left(\frac{4\pi}{\Lambda} x\right) + \ldots \tag{8}$$

$$a(x) = a_0 + a_1 \cos\left(\frac{2\pi}{\Lambda} x\right) + a_2 \cos\left(\frac{4\pi}{\Lambda} x\right) + \ldots . \tag{9}$$

If a reading beam strikes the sample more or less along the direction of the reference wave, some of the light is diffracted by the grating produced by the spatial variations in n and a into the direction of the now absent object wave. The diffracted beam is the holographic image of the object beam and the efficiency of this hologram η is defined as the intensity in the diffracted beam divided by the intensity in the reading beam. More complex holographic images can be viewed as being made up of linear combinations of n and a variations as represented in Eqs. (11) and (12) with various spatial periods Λ [10].

Kogelnik [8] has obtained the following expression for a plane wave incident on a holographic grating of thickness d

$$\eta = \exp\left(-\frac{2\bar{a}d}{\cos\theta}\right)\left[\sin^2\left(\frac{\pi n_1 d}{\lambda' \cos\theta}\right) + \sinh^2\left(\frac{a_1 d}{2\cos\theta}\right)\right] \qquad (10)$$

where $\bar{a}$ is the average absorption coefficient across the sample and λ' is the reading wavelength which may differ from the writing wavelength λ. This expression is valid under the following conditions:

(1) the modulation amplitude is independent of z

(2) the holograms are thick, $d >> \Lambda$

(3) the n and a modulations are sinusoidal

(4) the reconstruction beam strikes the sample at the Bragg angle for light of wavelength λ'.

The exponential factor in Eq. (13) accounts for the absorption of the reconstruction wave as it passes through the sample. The assumption that the modulation amplitude is independent of z is equivalent to assuming that this factor is nearly unity. Our

conclusions based on Eq. (13) are thus strictly valid only for optically thin samples. As we have previously shown [1] for short times even in optically thick samples, Eq. (13) is valid. Tomlinson [8] has treated the more complicated case of hologram formation in optically thick samples where the radiation intensity and hence the photochemistry are complicated functions of z and time [11].

The two terms inside the square bracket represent two different mechanisms of hologram formation. The first term describes hologram formation as a result of changes in the index of refraction. Holograms of this type are called *phase holograms*. The second term describes holograms resulting from changes in the absorption coefficient. These holograms are called *amplitude holograms*. It can be shown that the maximum theoretical efficiency for a thick amplitude hologram is 3.7%. On the other hand, thick phase holograms may approach efficiencies of 100% [6]. We will see below that the holograms observed in benzophenone are almost pure phase holograms [4].

B. Relationship Between Hologram Growth and Photochemistry

1. Phase Holograms

To relate the growth of the hologram to the underlying photochemical reaction, we must relate the changes in index of refraction and absorption coefficient to the variation in concentration of reactants and products. For phase holograms this is done by utilizing the Lorentz-Lorenz relationship between polarizability α and index of refraction [6,12]. Introducing a molar refraction R given by

$$R = \frac{4\pi}{3} A\alpha \tag{11}$$

this relationship can be expressed as:

$$\frac{n^2-1}{n^2+2} = \frac{\rho R}{M} \tag{12}$$

where ρ is the density of the polarizable species and M is its molecular weight. For an ideal mixture where one can neglect electronic interactions among the components, Eq. (12) becomes

$$\frac{n^2-1}{n^2+2} = \sum_i \frac{\rho_i R_i}{M_i} \tag{13}$$

where the sum is over all i components of the mixture.

For any one component the molar refraction $R_i(\omega)$ can be related to the oscillator strengths f_s^i of the various electronic transitions s for the i-th component [6]:

$$R_i(\omega) = \frac{4\pi}{3} \frac{Ae^2}{m} \sum_s \frac{f_s^i}{\omega_s^{i\,2} - \omega^2} \tag{14}$$

where ω_s^i is the frequency of the s-th transition in the i-th component of the mixture and where e and m are the electron charge and mass, respectively. Note that the molar refraction is a function of frequency. Equation (14) holds only in those frequency regions far away from absorption bands where one can neglect contributions from the imaginary part of the index of refraction. In most of the experimental situations that we have encountered, the interfering laser beams have been at the edge of an absorption band so that this approximation is valid. Should it be necessary one could, without difficulty, calculate the molar refractivity including damping.

Suppose that as a result of a chemical reaction the density or concentration of the i-th component changes by an amount $\Delta\rho_i$. When this change does not result in a large change Δn in the index of refraction with respect to n we may write the resulting change in the index of refraction as

$$\Delta n \cong \frac{(n^2+2)^2}{6n} \sum_i \frac{\Delta\rho_i}{M_i} R_i(\omega) . \tag{15}$$

Here M_i is the molecular weight of the i-th component. This result assumes that the chemical reaction only affects the concentrations or number densities of products and reactants and that there are no local changes in the structure of the system that might affect the overall density. The assumption is not appropriate for many holographic materials such as widely used dichromated gelatin where extensive local density changes occur as a result of the photochemistry [13].

Equation (15) is the key expression for calculating the change of the index of refraction as photochemistry proceeds. The density change $\Delta\rho_1$ for the starting material in the reaction can be related to its initial concentration at $t=0$ in moles/liter, C_o^1 and the concentration at time t, $C^i(t)$, of the i-th component by the expression:

$$\Delta\rho_1 = \left(\frac{C^1(t)}{C_o^1} - 1\right)\rho_o^1 \tag{16}$$

where ρ_o^1 is the initial density of component 1

$$\rho_o^1 = \frac{C_o^1}{1000} M_1 . \tag{17}$$

The photochemical products are assumed to have zero initial concentrations. The density charges for these components are given by

$$\Delta\rho_i = \frac{C^i(t)}{C_o^1}\,\rho_o^1 \tag{18}$$

where $i \neq 1$ and where ρ_o^i is determined by Eq. (17) with 1 replaced by i. The time dependence of $C^i(t)$ can be calculated from kinetic rate equations as will be discussed in Section IIID.

2. Amplitude Holograms

For amplitude holograms the time dependence of the efficiency depends on changes in the absorption coefficient of the various components $\alpha^i(\omega)$. This absorption coefficient is related to the molar extinction coefficient $\varepsilon(\omega)$ by the well-known expression [14]

$$\alpha^i(\omega) = 2.30\varepsilon^i(\omega)C^i\,. \tag{19}$$

To emphasize the relationship between the phase and amplitude hologram equations, we can define a quantity that we will call the molar absorption coefficient $S_i(\omega)$ by analogy with the molar refraction $R_i(\omega)$:

$$S_i(\omega) = \frac{\alpha^i(\omega)}{C^i} = 2.30\varepsilon^i(\omega)\,. \tag{20}$$

Just as for $R_i(\omega)$, $S_i(\omega)$ can be calculated knowing the oscillator strength f and the absorption line shape since [15]

$$f = \frac{2.33\times10^{-20}}{n}\int \varepsilon(\omega)\mathrm{d}\omega\,. \tag{21}$$

The change in absorption coefficient can then be written as a function of time in a manner similar to Eq. (20):

$$\Delta\alpha^1 = \left(\frac{C^1(t)}{C_o^1} - 1\right) C_o^1 S_1(\omega) . \tag{22a}$$

$$\Delta\alpha^i = \frac{C^i(t)}{C_o^1} \rho_o^1 S_i(\omega) \quad i \neq 1 . \tag{22b}$$

Then knowing the absorption spectra of the reactants, their concentration, and the kinetic rate equations one can evaluate the time dependent quantity $\Delta\alpha^i$.

IV. TIME DEPENDENCE OF HOLOGRAM GROWTH

A. General Remarks

In this section we will describe calculations of holographic growth curves using the general procedure outlined in Section III. Since we will use as an experimental example the hydrogen abstraction reaction of benzophenone in polymethylmethacrylate [4], we will choose parameters for our calculation appropriate for this photochemical reaction. The parameters used are gathered together in Table I. Some of these parameters will be discussed in more detail below.

Three general photochemical reaction schemes will be treated; a simple one-step reaction

$$A_1 \rightarrow A_2 ,$$

two parallel reactions

$$A_1 \rightarrow A_2$$

$$A_1 \rightarrow A_3 ,$$

and a consecutive reaction scheme

$$A_1 \rightarrow A_2 \rightarrow A_3 \, .$$

This last case corresponds to the situation actually observed for benzophenone.

B. One-Step Reaction Scheme; $A_1 \rightarrow A_2$

The one-step reaction scheme is the simplest photochemical reaction sequence one can consider. It corresponds to the situation actually observed for dimethyl-s-tetrazine and camphorquinone [1]. The time dependence for the build-up of A_2 and depletion of A_1 is exponential:

$$C^1(t) = C_o^1 e^{-kt} \tag{23a}$$

$$C^2(t) = C_o^1 - C^1(t) \, . \tag{23b}$$

These expressions can be used to calculate Δn or Δa using Eqs. (15) and (22), respectively, provided that one knows k. The calculation of k for one and two-photon processes has been discussed in a previous publication [1b]. If n indicates the number of photons involved in the photochemical reaction, it has been found that:

$$k = \xi I^n \tag{24}$$

where

$$\xi = (2303.)\phi\varepsilon_1 \quad \text{for } n = 1 \tag{25}$$

$$= (2303.)^2\phi\varepsilon_1\varepsilon_2\tau \quad \text{for } n = 2 \, . \tag{26}$$

Since the benzophenone hydrogen abstraction reaction is a two-photon process [4,16], we will only consider the $n=2$ case below. However, except for the intensity dependence, there is little difference between holographic growth curves produced by one and two-photon processes. ε_1 is thus chosen to be appropriate for the $S_0 \rightarrow S_1$ transition of benzophenone. The second photon is absorbed by the benzophenone lowest triplet state, $T_1 \rightarrow T_n$, and we use a value of ε_2 appropriate to this transition [17]. τ is chosen to be equal to the benzophenone triplet state lifetime.

To actually calculate the hologram efficiency from Eq. (10), we need to know how the photochemistry described by Eqs. (23) modifies the index of refraction and/or the absorption coefficient. We will first consider a pure phase hologram produced by index of refraction changes. Equation (14) relates the transition oscillator strength to the molar refractivity. In Table II we have listed the transition oscillator strengths and wavelengths for A_1 which we assume to be benzophenone. A_2 is assumed to be the intermediate formed after hydrogen abstraction. This intermediate has a strong absorption in the same spectral region as the benzophenone lowest $n\pi^*$ singlet state absorption. This is reflected in Table II by the increased oscillator strength for A_2 in this region. Values for $R^i(\omega)$ calculated using these parameters are shown in Figure 3 as a function of wavelength. (The curve for A_3 will be discussed below in Subsection D.) From the curves in Figure 3 we extract the values of R_1 and R_2 for the wavelength at which the holograms are to be read, 350 nm in the present case. These values are listed in Table I.

With these values and Eq. (15) one can calculate the index of refraction change provided one knows the laser intensity. Of course the laser intensity will vary across the sample in a manner described by Eq. (1). In Figure 4 the variation of Δn across the

benzophenone/PMMA sample as a result of the light intensity variation is shown at several times during the process of a two-photon photochemical reaction. Curves for the Δn variation of a one-photon photochemical system look qualitatively similar. Because we have chosen the fringe visibility V to be 1.0, the point at a distance 0.5 in the figure receives no light and thus Δn will always be zero at this point. In actual experiments V is less than 1.0 because of inequalities in the intensities of the interfering beams, motion of substrate and beams, and variations in laser wavelength.

To calculate the hologram efficiency using Eq. (10), one needs to know n_1 as defined in Eq. (8). Equation (8) is actually a Fourier series expansion of the spatially varying index of refraction and n_m is one of the coefficients in the expansion. It may, therefore, be obtained from the expression

$$n_m = \frac{1}{\pi}\int_0^{2\pi} n(X)\cos mX\,dX \tag{27}$$

where

$$X = \frac{2\pi x}{\Lambda}.$$

The integral in Eq. (27) may be evaluated using $n(X)$ determined at various times during the hologram growth. One can substitute these values into Eq. (10) to obtain a time dependent hologram efficiency η. First order holographic growth curves generated in this way are shown in Figure 5. The first order curves are obtained using $m=1$ in Eq. (27). To correlate these curves with the progress of the photochemistry, we note that the rate k for an intensity of 1 W/cm^2 is 0.032 sec^{-1}. The maximum in the hologram efficiency occurs near the time $t=1/k$ as Figure 5 shows. In Figure 5 we also illustrate the effects of decreasing the fringe visibility V on the shape of the growth curves. Decreasing V

results in an overall lowering of the maximum attainable efficiency as shown in Figure 5(a). It also tends to cause a more rapid washing out of the hologram at longer times as shown in Figure 5(b). Because the shape of the growth curve is sensitive to changes in V and because V is not a parameter that is easily accessible experimentally, we have chosen to fix V at 1.0 and compare calculated and experimental growth curves qualitatively only. Careful control of the parameter will be necessary if one wants to fit the calculated hologram growth curve to the experimental one.

If one sets m in Eq. (27) equal to 2, one obtains the coefficient n_2. This coefficient can be used in Eq. (10) to calculate the growth of the second order hologram that appears displaced from the reference beam by an angle 4θ. It is sometimes convenient to use higher order holograms to follow the photochemistry since these holograms occur spatially distinct from the object and reference beams and can be monitored without turning off the object beam [1]. The growth of a second order hologram is compared to that of a first order hologram in Figure 6 for a simple one-step reaction scheme. The curves are normalized in the figure to a maximum efficiency of 1.0 for easier comparison of their shapes. The actual maximum efficiency of the second order hologram is 0.003 compared to a value of 0.009 for the first order hologram. In addition to being weaker, Figure 6 indicates that the second order hologram reaches its maximum efficiency much more slowly as well.

In previous publications [1] we have developed an equation that describes the hologram efficiency as a function of time for early times in the hologram growth

$$\eta = a(I)t^2 \tag{28}$$

where $a(I)$ has the functional form

$$a(I) = bI^{2n} \tag{29}$$

and where b is a constant. This form is convenient for analyzing experimental data. It relies for its validity on two approximations. First and most frequently satisfied, the argument of the sine in Eq. (10) must satisfy the inequality

$$\frac{\pi n_1 d}{\lambda' \cos \theta} << 1 .$$

This inequality is satisfied during the early stages of the hologram growth when the efficiency is low. Equation (28) also assumes that there is no significant depletion of the concentration of original molecules A_1. This is true provided

$$t << 1/k .$$

To see how well this approximation describes the hologram growth we have plotted the function η/t^2 as a function of time in Figure 7. If Eq. (28) were strictly valid η/t^2 would be independent of time. In the figure one can see that this approximation is roughly true for times shorter than 3 sec. This time should be compared to $1/k$ which for the parameters used here is 31s.

It is clear from the figure that one wants to measure the quadratic growth rate $a(I)$ at very early times in the hologram growth process. Since time enters the hologram efficiency equations only via the kinetic expressions Eq. (23), the actual shape of the holographic growth curve is independent of k when η is plotted vs. a dimensionless time $T=kt$. This means that if one measures an average $a(I)$ over the same efficiency range the average value of $a(I)$ found will be proportional to k even though strictly speaking

$a(I)$ is not itself a constant. In this way plots of $a(I)$ vs. I can be used to measure the order of the photochemical reaction n even when the plots are made over time spans where $a(I)$ is not strictly constant. Of course, another way of obtaining a more accurate value for $a(I)$ would be to add higher order terms to Eq. (28) and fit the hologram growth curve to this multiparameter expression. In view of the accurate values of $a(I)$ obtained experimentally using the first method [1,4], this more complex method does not seem necessary.

We next turn to a consideration of pure amplitude holograms arising from changes in the absorption coefficient Δa of the sample. As we have shown in Eqs. (22), Δa^i for the i-th component of the system can be obtained knowing the molar absorption coefficient $S_i(\omega)$. To calculate $S_i(\omega)$ we need to know the value of $\varepsilon_i(\omega)$ at the frequency of interest ω. In our calculation we will assume the electronic transition oscillator strengths and wavelengths given in Table II. We will also assume that each of the electronic transitions is concentrated in a Gaussian line of 50 nm width centered at the appropriate wavelength given in the table. Values of $S_i(\omega)$ calculated in this way are shown in Figure 8. The component A_3 will be discussed in Section IVD. In this way the following S_i values are obtained at a wavelength of 350 nm:

$$S_1 = 372.62$$

$$S_2 = 2924.5 .$$

Using these values one can calculate the amplitude holographic growth curve. When this is done one obtains curves with shapes identical to the curves shown in Figure 5. The maximum efficiency obtained by the amplitude holograms in this case is 4×10^{-7}. This

should be compared to a maximum phase hologram efficiency of 0.009. The maximum amplitude hologram efficiency is small because the absorption coefficient of the 200μ, 0.03 mole/l sample of benzophenone in PMMA used as a model for these calculations is small. Clearly in this case the phase hologram is dominant. Since the phase hologram is dominant in the benzophenone case that we have chosen as an experimental example, we will not discuss amplitude hologram formation anymore. It is straightforward to add contributions from amplitude holograms in those cases where it might be necessary.

C. Parallel Reaction Scheme; $A_1 \rightarrow A_2$, $A_1 \rightarrow A_3$

The solution of the kinetic equations appropriate to the reaction scheme

$$A_1 \xrightarrow{k_1} A_2$$

$$A_1 \xrightarrow{k_2} A_3$$

are straightforward [7]. With the definitions

$$T = k_1 t$$

$$K = k_2/k_1$$

one obtains the following expressions for the time dependence of the concentrations:

$$X_1 = \frac{C^1}{C_o^1} = e^{-(1+K)T} \tag{30a}$$

$$X_2 = \frac{C^2}{C_o^1} = \frac{1}{(1+K)}\left(1 - e^{-(1+K)T}\right) \tag{30b}$$

$$X_3 = \frac{C^3}{C_o^1} = KX_2 . \qquad (30c)$$

Note that for this reaction the ratio X_3/X_2 is always a constant K. This means that the index of refraction changes from that of the background value n_o plus a contribution from A_1 to a contribution from A_1 plus a contribution from A_2 and A_3. Since the ratios of A_2 and A_3 contributions always remain the same, the hologram growth is qualitatively identical to the simple one step reaction scheme treated in the preceding subsection. It is thus impossible from the shape of the hologram growth curves to distinguish between this reaction mechanism and the one step mechanism of the previous subsection.

When the two parallel reactions involve different numbers of photons and thus have different intensity dependence one can, by plotting $a(I)$ vs. I, distinguish this parallel reaction scheme from other schemes. This is illustrated in Figure 9 for the case where the first reaction $A_1 \rightarrow A_2$ depends linearly on intensity and the second step $A_1 \rightarrow A_3$ is quadratic. The parameters used in the calculation are given in Table I assuming a hologram writing and reading wavelength of 350 nm. The value of R_3 chosen for A_3 will be discussed in Subsection D. Here we only note that in the second reaction $A_1 \rightarrow A_3$ the molar refractivity decreases while in the reaction $A_1 \rightarrow A_2$ it increases. This results in an interesting hologram cancellation effect that we will discuss below. In Figure 9 it has the effect of causing the 'kink' in the plot of $a(I)$ vs. I as the system goes from a behavior at low intensities dominated by the first reaction to a behavior at higher intensities dominated by the second reaction. Of course when both reactions result in changes in refractive index of the same sign, the 'kink' is not present and one passes smoothly from low to high intensity regimes. In this context holographic techniques may be useful in

identifying photochemical systems in which the products may vary depending on the intensity of the exciting light. Examples of such systems have recently been discussed [18].

Since in the present embodiment of the holographic experiments the reactions occur in the solid state, another variation of the parallel reaction scheme must be considered. In this variation

$$\begin{aligned} A_1 &\xrightarrow{k_1} A_2 \\ A_1' &\xrightarrow{k_2} A_3 . \end{aligned}$$

Here molecule A_1 may sit in two different reactive sites. In one of the sites A_2 is the photochemical product and in the other A_3 is produced. These reactions are completely independent of each other. The resulting kinetic expressions are simply two sets of equations identical to Eqs. (23).

In the case where the hologram is written and read at 350 nm, where k_2/k_1 is 0.01 and where both steps are quadratic one obtains the curve shown in Figure 10(a). Initially the hologram is produced as a result of the rapid reaction $A_1 \rightarrow A_2$. As A_1 molecules are depleted, however, the hologram due to this reaction begins to disappear. In addition the $A_1' \rightarrow A_3$ reaction becomes increasingly important. Recall from the discussion above that production of A_3 results in an index of refraction change different in sign from the one resulting from A_2 production. The initial effect of the slow increase in A_3 concentration is to reduce the efficiency of the A_2 hologram. As Figure 10(a) shows, the hologram goes through zero efficiency and then increases again as the A_3 concentration rises further.

If one uses the parameters for the molar refractivity appropriate for reading the hologram at 514 nm (shown in Figure 3), one obtains the hologram growth curve shown in Figure 10(b). Here the hologram is being produced at 350 nm but read at 514 nm. Since at this reading wavelength, A_2 and A_3 result in molar refractivity changes of the same sign, the second hologram growth reinforces the first hologram. As a consequence the efficiency does not return to zero as it does at 350nm.

The actual behavior observed for hologram formation resulting from the hydrogen abstraction of benzophenone in PMMA [4] is shown in Figure 11. The behavior observed corresponds at least qualitatively to that expected from the theoretical considerations discussed above. Measurements of the absorption spectrum of the benzophenone/PMMA system at various times during the progress of the photochemistry reveals, however, that this is not what is happening [4]. The reaction scheme for benzophenone will be discussed in the next subsection.

D. Consecutive Reaction Scheme; $A_1 \rightarrow A_2 \rightarrow A_3$

For the consecutive reaction scheme

$$A_1 \xrightarrow{k_1} A_2 \xrightarrow{k_2} A_3$$

again using the definitions

$$T = k_1 t$$

$$K = k_2/k_1$$

one obtains the following expressions for the time dependent concentrations [7]

$$X_1 = \frac{C^1}{C_o^1} = e^{-t} \tag{31a}$$

$$X_2 = \frac{C^2}{C_o^1} = \frac{1}{K-1}\left(e^{-T} - e^{-KT}\right) \tag{31b}$$

$$X_3 = \frac{C^3}{C_o^1} = 1 + \frac{1}{1-K}\left(Ke^{-T} - e^{-KT}\right). \tag{31c}$$

Since this is the reaction scheme that is appropriate for describing the benzophenone photochemistry in PMMA, we will briefly discuss that photochemistry [4]. Considering only the products that live long enough to produce holograms with lifetimes of minutes or longer, the reaction can be written:

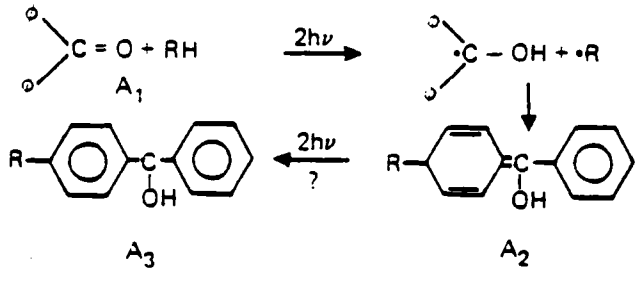

The final product A_3 is speculative but does seem to be consistent with the observed changes in the absorption spectrum. To calculate the index of refraction changes we use the above reaction scheme as a model. The parameters chosen for the absorption characteristics are presented in Table II. The values for benzophenone are well known [19]. The values for A_2 are chosen by replacing the benzophenone $n\pi^*$ transition at 338 nm by a stronger $\pi\pi^*$ transition at 333 nm. This is in agreement with the observed spectral changes that show an intense band at 333 nm gradually growing in to replace the benzophenone absorption in this region. The final product is assumed to have an absorption spectrum similar to that of diphenylmethane [20] which in turn has been shown to resemble twice the spectrum of toluene [21].

These parameters result in the previously discussed molar refractivity curves shown in Figure 3. A crucial feature of these curves is the cross-over between the A_1 and A_2 curves at about 390 nm. Replacement of benzophenone (A_1) by A_2 results in an increase of molar refractivity at 350 nm but a decrease at 514 nm. The final product A_3 always results in a decrease of molar refractivity when compared to that of A_1. The consequences of this cross-over of the index of refraction curves for the parallel reaction scheme has been shown in Figure 10. In Figure 12 the hologram growth curves are shown for the consecutive reaction scheme and it can be seen that similar growth curves are obtained. Both parallel and consecutive reaction schemes are in qualitative agreement with the experimentally observed growth curves shown in Figure 11. It should be noted that none of the parameters used in the calculation of the hologram growth curves and listed in Table I have been chosen to fit the experimental curves. One could achieve even better correspondence between calculated and experimental curves by adjusting the input parameters, particularly the molar refractivities and the fringe visibility.

The distinction between parallel and consecutive reaction schemes can be made in the case of benzophenone/PMMA photochemistry by examining the absorption spectrum as the reaction proceeds. If the parallel reaction scheme were appropriate for describing the photochemistry, the absorption at 333 nm due to A_2 would remain even as the A_3 hologram grew. This does not occur. As the A_3 absorption grows the A_2 absorption disappears [4] clearly indicating that the reaction proceeds by a consecutive scheme.

V. CONCLUSION

In this paper we have presented a general framework for calculating holographic growth curves provided one knows and can solve the kinetic equations for the appropriate

photochemistry. Three kinetic schemes have been used as examples; a simple one-step reaction, a parallel reaction scheme resulting in two different products, and a two-step consecutive reaction scheme. More complex schemes can be treated by straightforward extension of the technique outlined.

It has been shown that the parallel and the simple one-step reaction schemes cannot be distinguished from each other by analysis of the shapes of the holographic growth curves alone. Additional experimental information is necessary. It has also been shown that the two-step consecutive reaction scheme yields growth curves similar in shape to curves obtained from a parallel reaction scheme where the reactant molecules sit in two different reactive sites and yield different products. These two schemes can be distinguished from an analysis of the time-dependent absorption spectrum. For benzophenone in PMMA the consecutive reaction scheme has been shown to be operative.

ACKNOWLEDGMENTS

The authors express their indebtedness to G. C. Bjorklund for his important assistance in solving many of the mysteries of holography. We are also grateful to D. C. Alvarez for his help in preparing the samples used in these experiments and to R. W. Martin for developing the lab automation programs used in our experiments. This work was supported in part by the Office of Naval Research.

Table I

Parameters Used in Calculating Holographic Growth Curves

Parameter	Value	Parameter	Value
n_o	1.5	τ	1 msec
ϕ	1.0	ϵ_1	140 l/mole•cm
I	1 W/cm^2	ϵ_2	5000 l/mole•cm
V	1.0	d	200μ
M_1	182.21	K	0.01
$M_2 = M_3$	183.21	C_o^1	0.03mole/l
θ	0.01 rad.		
λ	350 nm	514 nm	
R_1	27.447	19.249	
S_1	372.62	—	
R_2	37.727	16.987	
S_2	2924.5	—	
R_3	14.043	11.347	
S_3	0.00003	—	

Table II

Wavelength and Oscillator Strengths
for Species Involved in Benzophenone Photochemistry

Species	Wavelength (nm)	Oscillator Strengths
Benzopheone[a] (A_1)	338 250 206 189	0.007 0.37 0.56 1.14
A_2[b]	333 206 189	0.100 0.56 1.14
A_3 (toluene $\times 2$)[c]	271 214 191	0.008 0.021 0.713

[a]Reference 19

[b]Estimated from experiment, see Reference 4

[c]Reference 21

REFERENCES

1. a) D. M. Burland, G. C. Bjorklund, and D. C. Alvarez, J. Am. Chem. Soc. **102**, 7117 (1980).

b) G. C. Bjorklund, D. M. Burland, and D. C. Alvarez, J. Chem. Phys. **73**, 4321 (1980).

2. Chr. Bräuchle, D. M. Burland, and G. C. Bjorklund, J. Am. Chem. Soc. **103**, 2515 (1981).

3. G. C. Bjorklund, Chr. Bräuchle, D. M. Burland, and D. C. Alvarez, Optcs L. **6**, 159 (1981).

4. Chr. Bräuchle, D. M. Burland, and G. C. Bjorklund, J. Phys. Chem. **85**, 123 (1981).

5. W. J. Tomlinson, E. A. Chandross, R. L. Fork, C. A. Pryde, and A. A. Lamola, Appl. Opt. **11**, 533 (1972); R. L. Kurtz and R. B. Owen, Opt. Eng. **14**, 393 (1975); R. A. Bartolini, H. A. Weakliem, and B. F. Williams, Opt. Eng. **15**, 99 (1976); R. A. Bartolini, Proc. Soc. Photo Opt. Inst. Eng. **123**, 2 (1977); R. G. Zech, *ibid.*, **177**, 56 (1979); P. Hariharan, Opt. Eng. **19**, 636 (1980).

6. W. J. Tomlinson and E. A. Chandross, Adv. Photochem. **12**, 201 (1980).

7. Z. G. Szabo, in *The Theory of Kinetics*, edited by C. H. Bamford and C. F. H. Tipper (Elsevier, Amsterdam 1969), pp. 1-80.

8. H. Kogelnik, Bell System Tech. J **48**, 2909 (1969); W. J. Tomlinson, Appl. Opt. **11**, 823 (1972); **14**, 2456 (1975).

9. H. M. Smith, *Principles of Holography* (Wiley-Interscience, New York 1969), pp. 158-171.

10. Reference 9, pp. 13-24.

11. E. L. Simmons, J. Phys. Chem. **75**, 588 (1971); H. Mauser, Z. Naturforsch. **22b**, 569 (1967); D. M. Burland and D. Haarer, IBM J. Res. and Dev. **23**, 534 (1979).

12. R. W. Ditchburn, *Light* (Academic Press, London 1976), pp. 547-553.

13 .B. J. Chang and C. D. Leonard, Appl. Opt. **18**, 2407 (1979); B. J. Chang, Opt. Eng. **19**, 642 (1980).

14. J. B. Birks, *Photophysics of Aromatic Molecules* (John Wiley, London 1970), pp. 46-47.

15. Reference 14, p. 51.

16. H. Murai and K. Obi, J. Phys. Chem. **79**, 2446 (1975).

17. R. Bensasson and E. J. Land, Trans. Far. Soc. **67**, 1904 (1971).

18. N. J. Turro, M. Aikawa, J. A. Butcher, and G. W. Griffin, J. Am. Chem. Soc. **102**, 5128 (1980); K. Yokoyama, J. Nakamura, T. Kobayashi, and S. Nagakura, Bull. Chem. Soc. Japan **53**, 3474 (1980).

19. S. Trovato, F. Zuccarello, G. Favini, and A. Millefiori, Spect. Acta **32A**, 351 (1976).

20. *UV Atlas of Organic Compounds* (Buttersworth, London 1966), Vol. II.

21. F. Marschner, Tet. **31**, 2303 (1975).

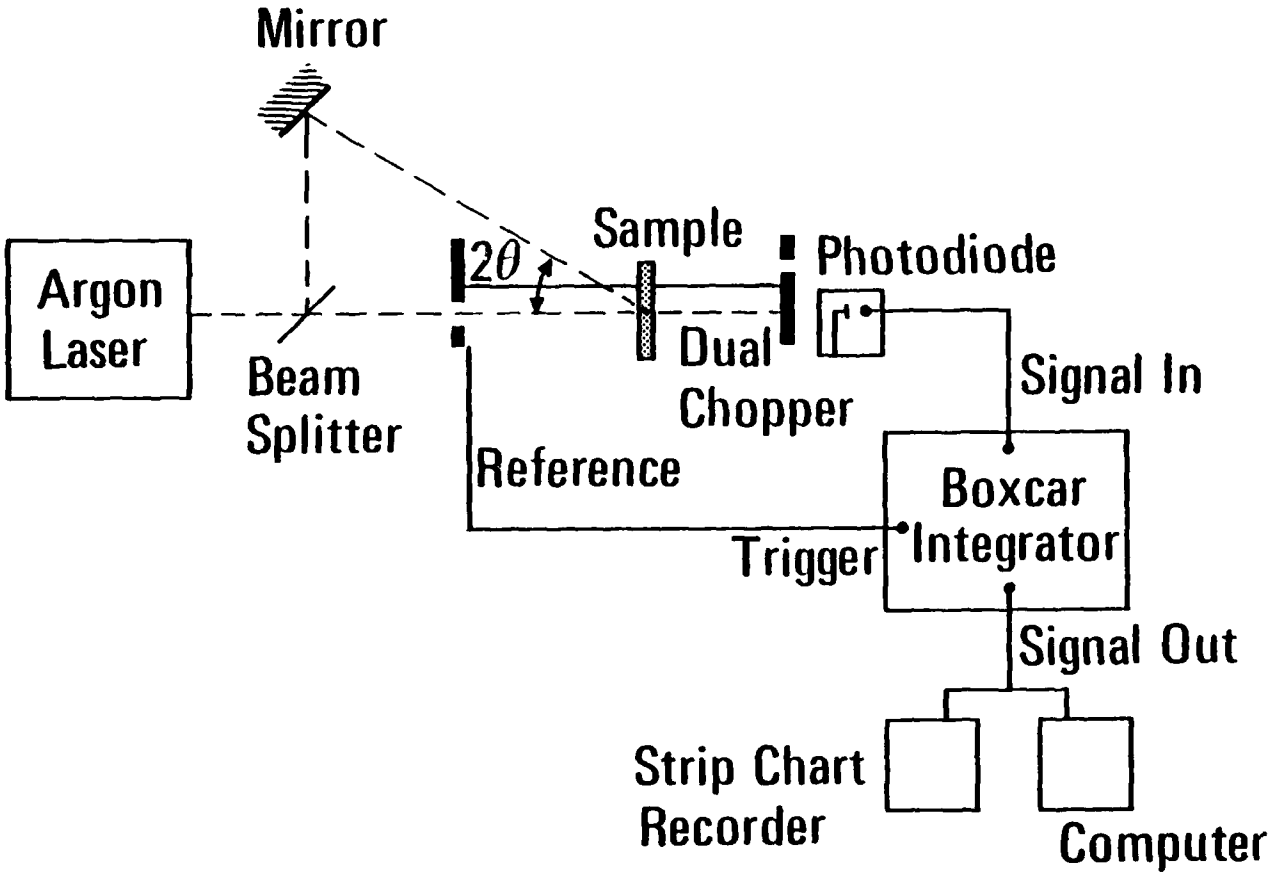

Figure 1. One of the experimental arrangements used to record the holographic growth curves.

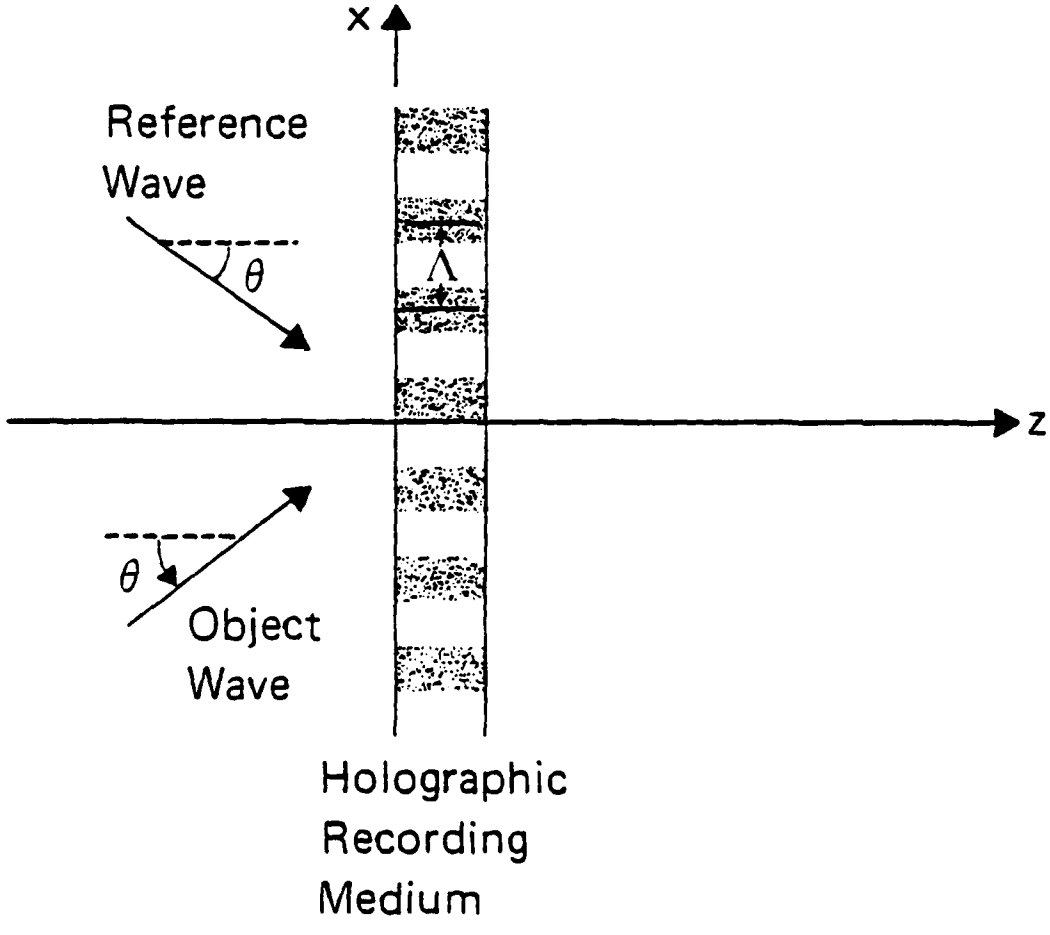

Figure 2. The formation of a hologram in a recording medium by the interference of an object and a reference beam. The darkened areas in the recording medium indicate the regions where the two beams destructively interfere and little photochemistry is produced. The lighter areas are regions of constructive interference. Λ is the fringe spacing and θ is the angle that each beam makes with the normal to the recording medium surface.

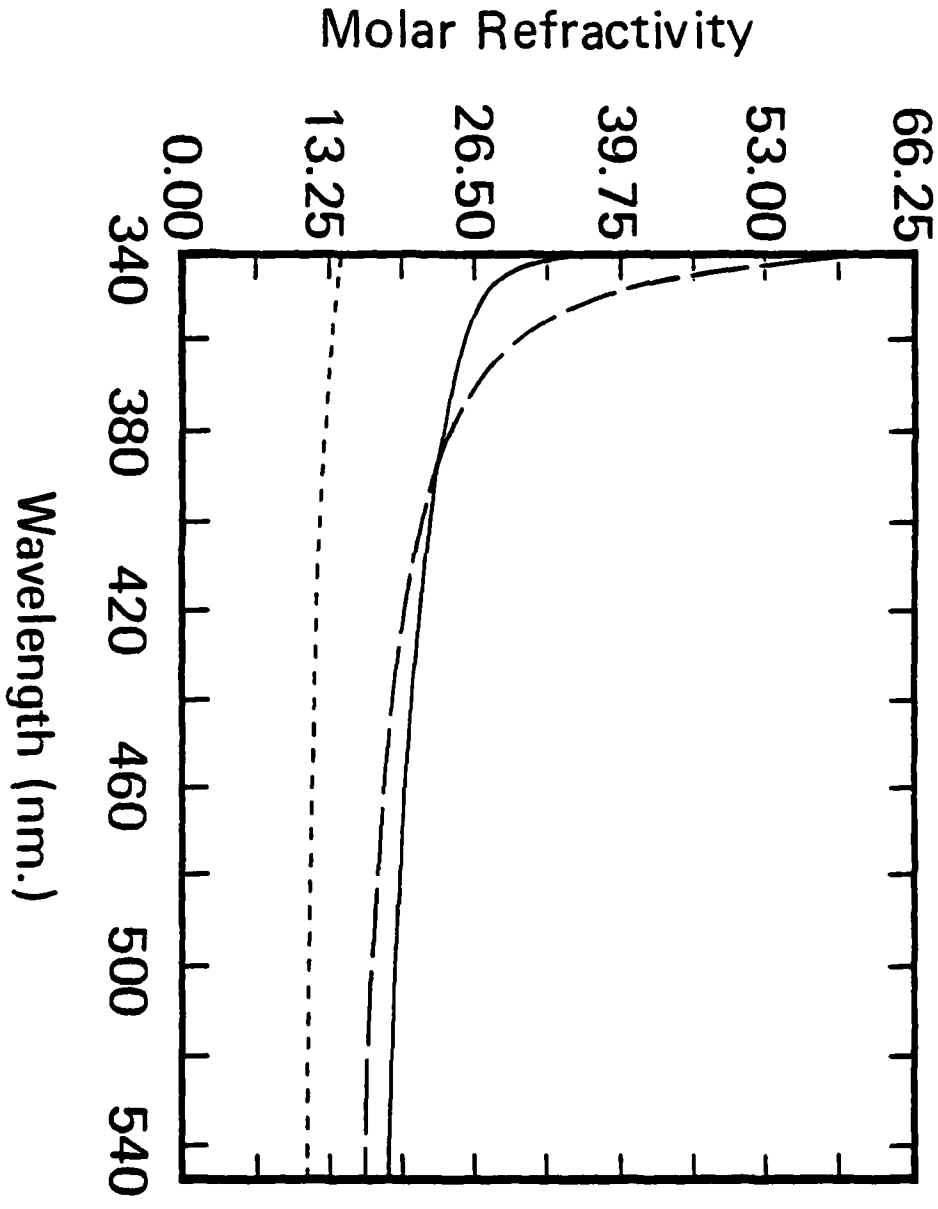

Figure 3. Molar refractivity as a function of wavelength calculated using the parameters in Table I. The three curves are for the three species involved in the benzophenone photochemistry. —— A_1 (benzophenone), — — — A_2, ----- A_3.

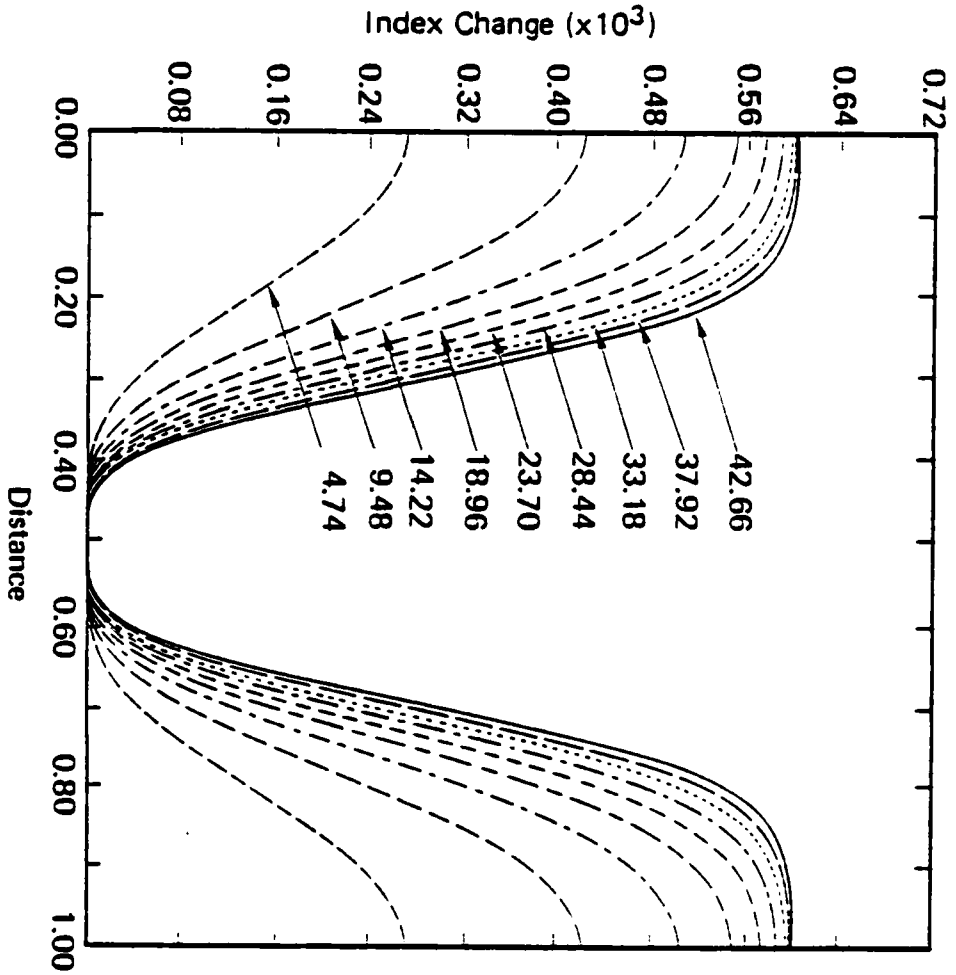

Figure 4. The index of refraction change as a function of distance for a one-step hologram involving the absorption of two photons, $A_1 \xrightarrow{2h\nu} A_2$. The various curves are for different times during the hologram growth and these times are indicated in seconds on the figure. The distance is in units of the fringe spacing Λ. A fringe visibility V of 1 has been assumed.

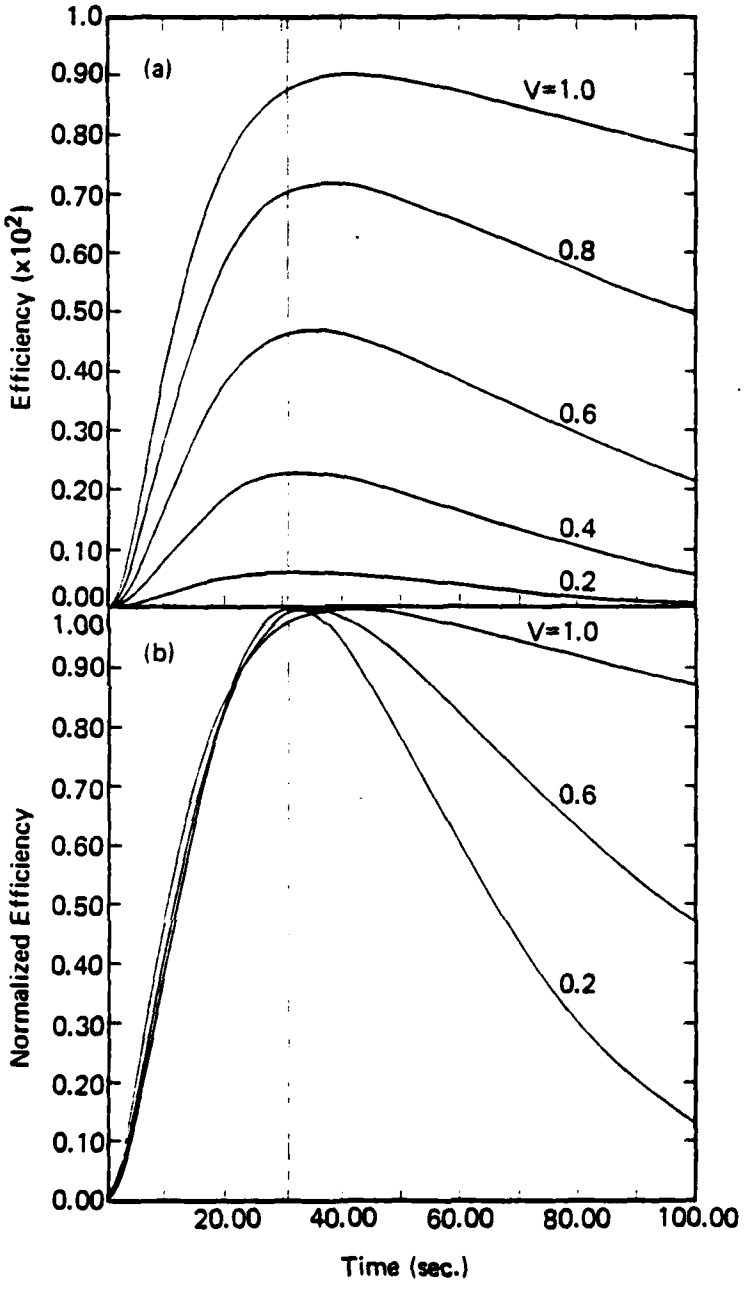

Figure 5. Hologram growth curves for a one-step, two-photon reaction using various values for the fringe visibility V. a) Efficiency vs. time indicating the decrease in maximum efficiency as the fringe visibility decreases. b) Normalized efficiency vs. time showing the change in shape of the hologram growth curve as the fringe visibility changes. The dotted vertical line notes the time at which $t=1/k$ where k is the reaction rate.

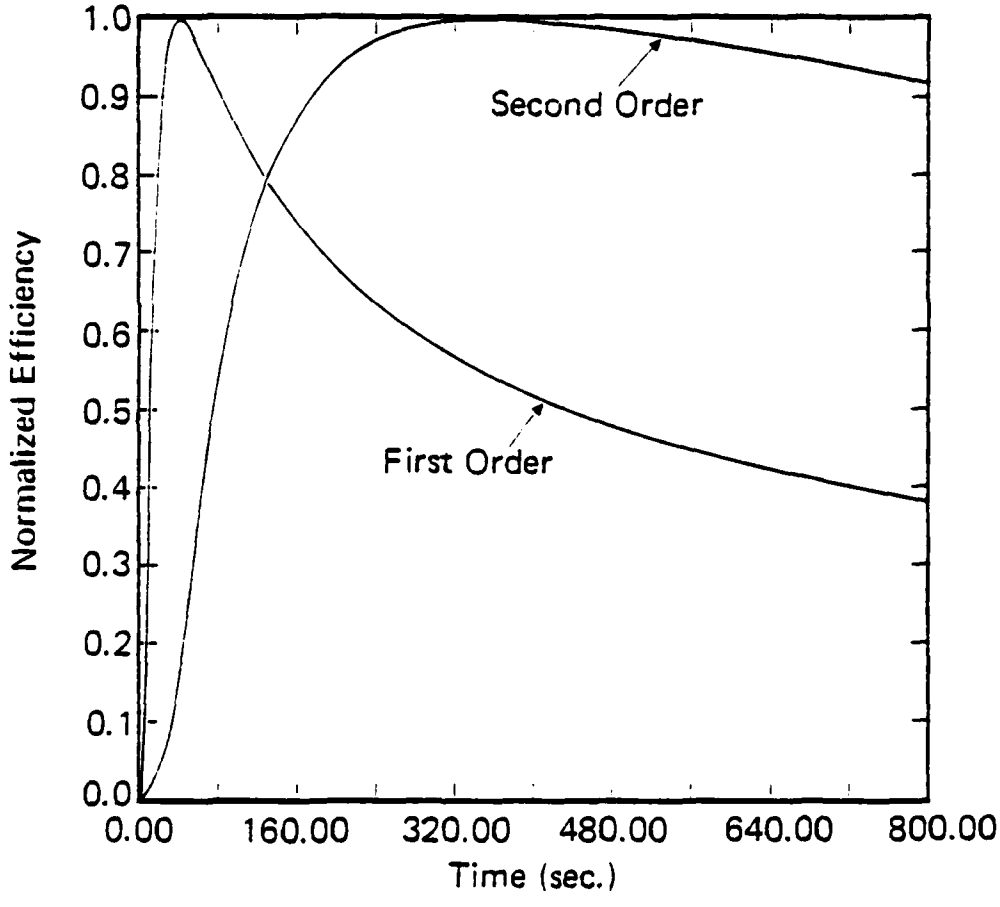

Figure 6. Hologram growth curves for first and second order holograms. Both curves have been normalized to maximum efficiencies of unity. In both cases a fringe visibility V=1 was assumed.

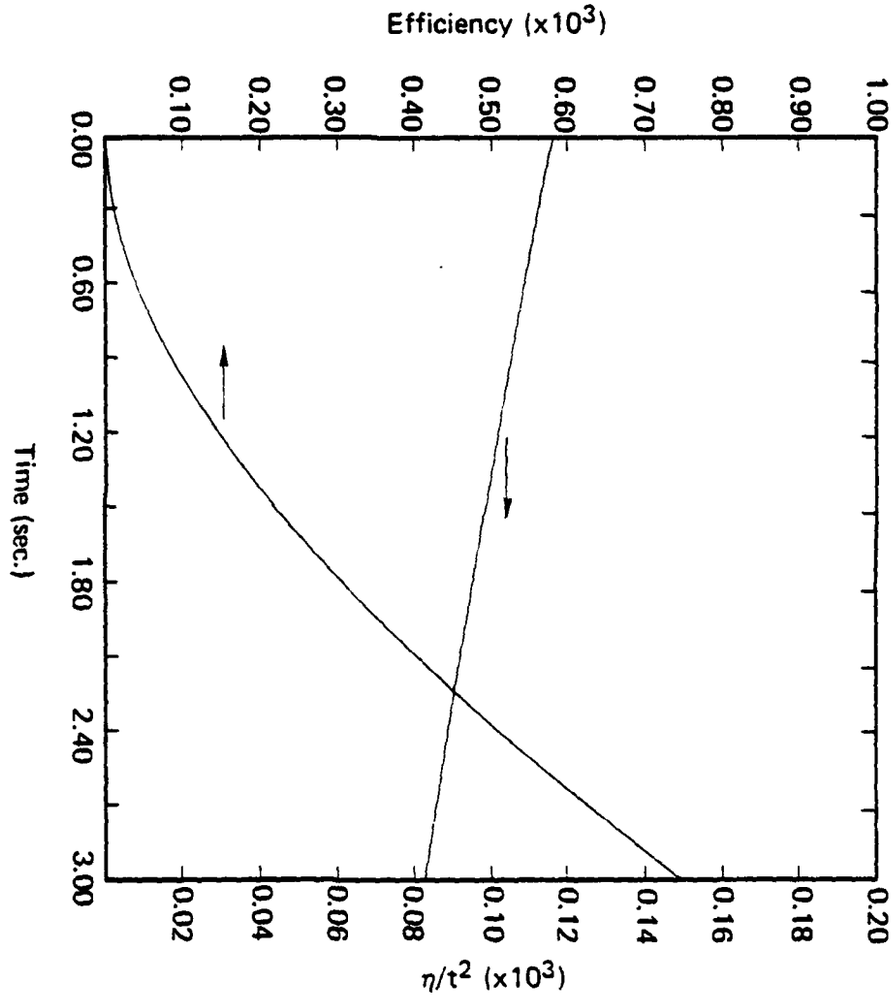

Figure 7. Hologram growth curve and $a(I)=\eta/t^2$ as a function of time.

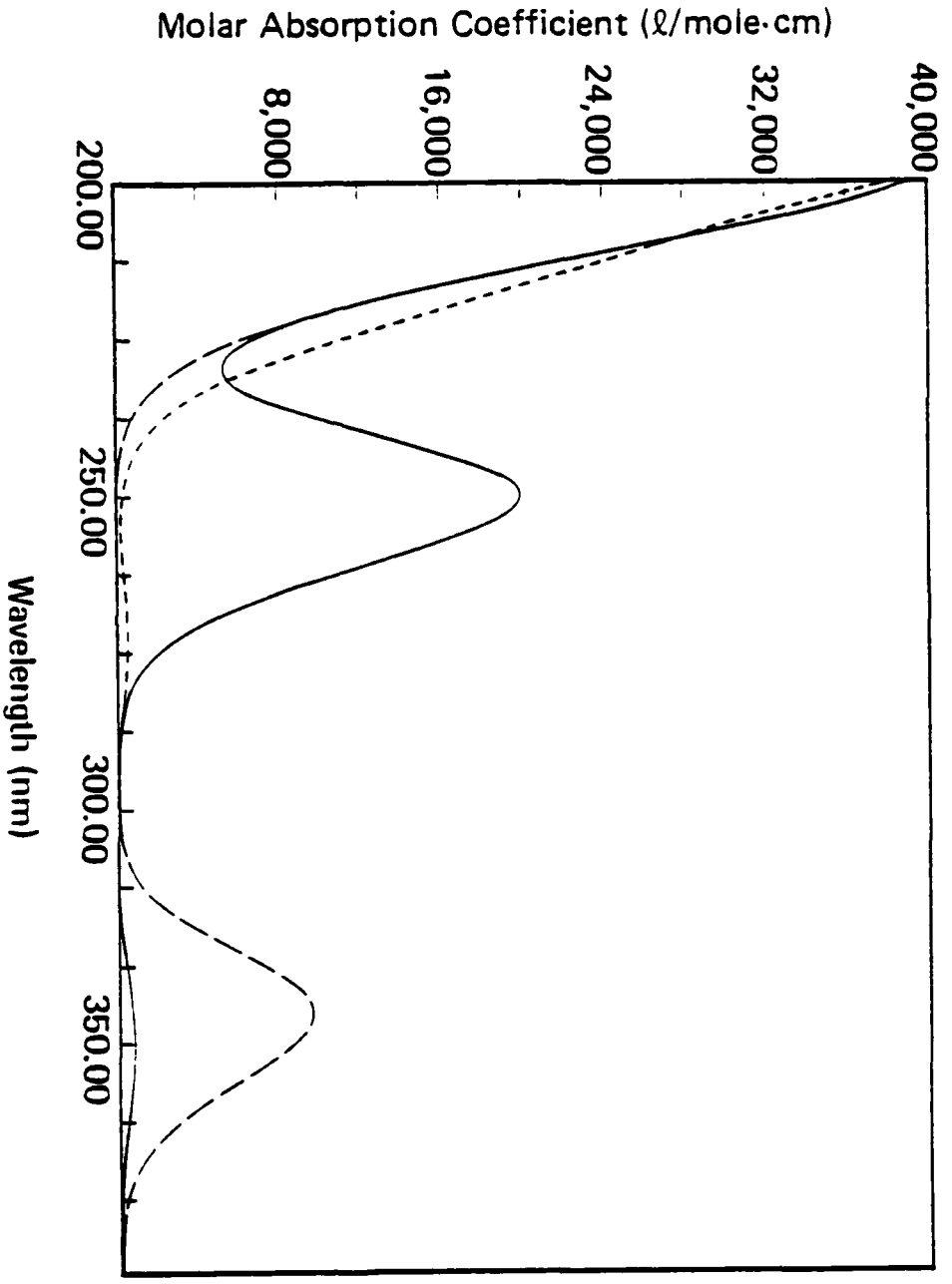

Figure 8. Molar absorption as a function of wavelength calculated using the parameters in Tables I and II. The curves are for the species A_1 (——), A_2 (— — —), and A_3 (-----).

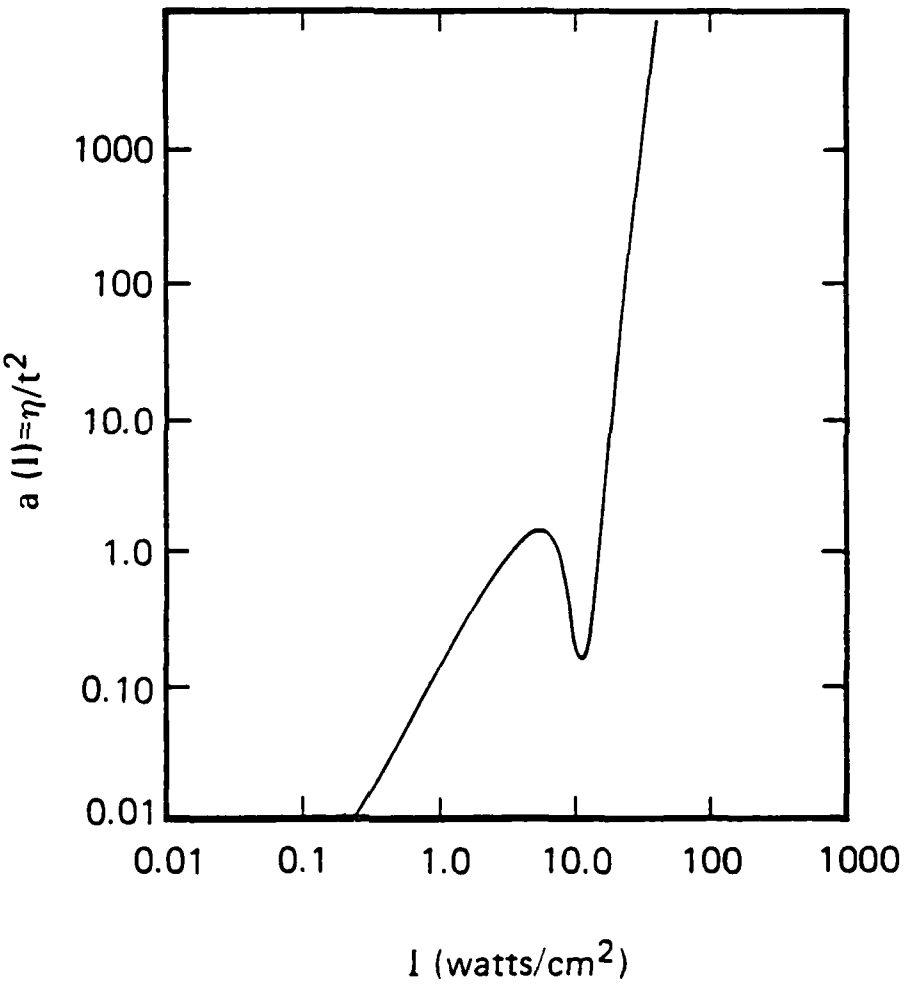

Figure 9. $a(I)$ vs. laser intensity calculated for a system undergoing two parallel reactions. One of the reactions is a one-photon process and the other requires two photons.

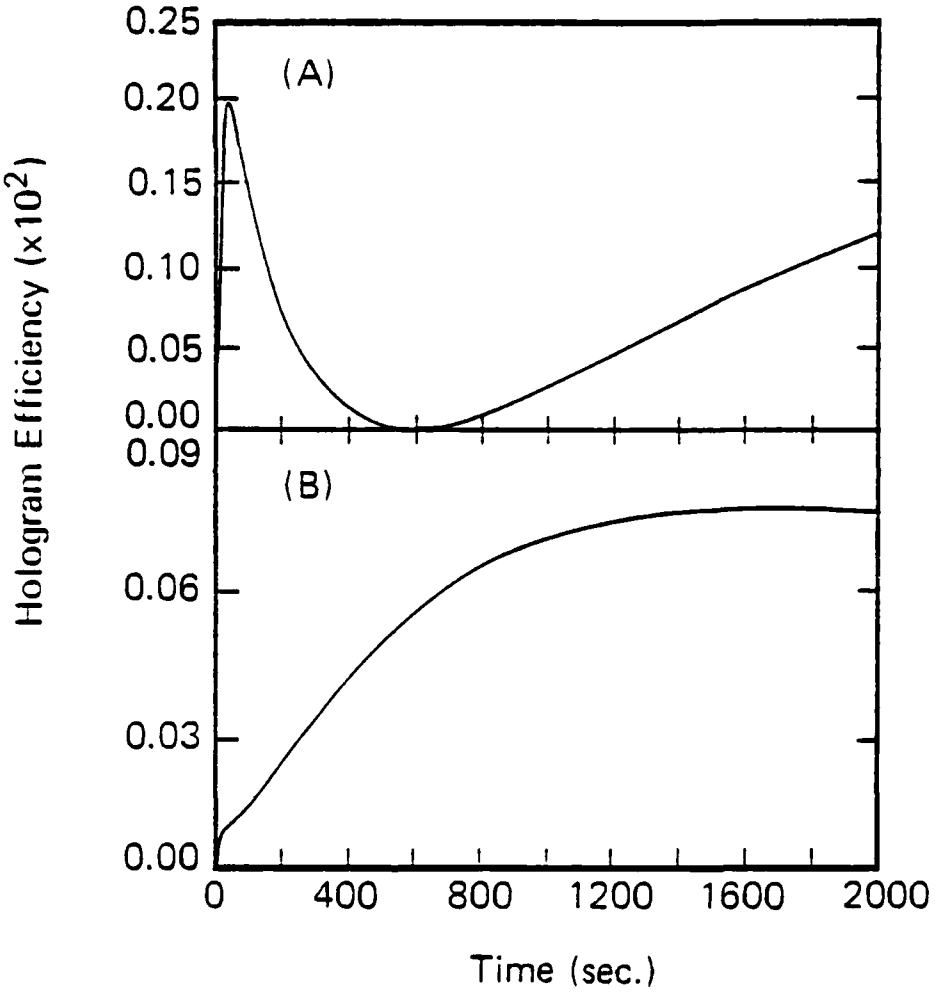

Figure 10. Calculated hologram efficiency vs. time for the parallel reaction scheme

$$A_1 \xrightarrow{2h\nu} A_2$$

$$A_1^1 \xrightarrow{2h\nu} A_3 .$$

a) Hologram produced and read at 350 nm. b) Hologram produced at 350 nm and read at 514 nm.

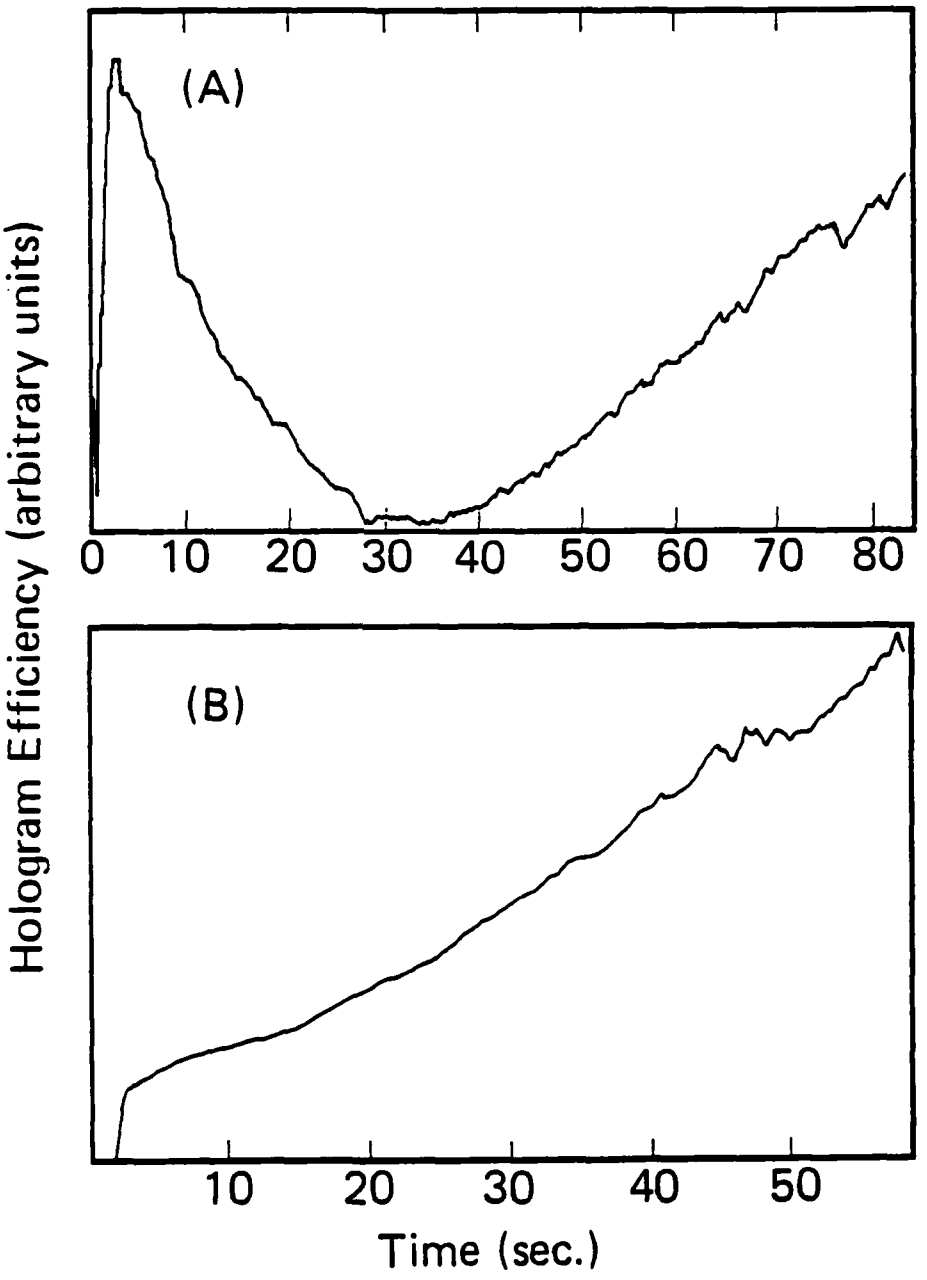

Figure 11. Experimental hologram efficiency vs. time for a 250μ thick sample of 5% by weight benzophenone in PMMA. a) Hologram produced and read using Ar^+ laser UV lines with a power density of 0.96 W/cm^2 in each laser beam. b) Hologram produced using Ar^+ laser UV lines with a power density of 0.73 W/cm^2 per beam. The hologram was read at 514.5 nm with a second Ar^+ laser with a power of 1.2 mW. Note that the start of the hologram growth has been shifted from zero time to make it more readily visible.

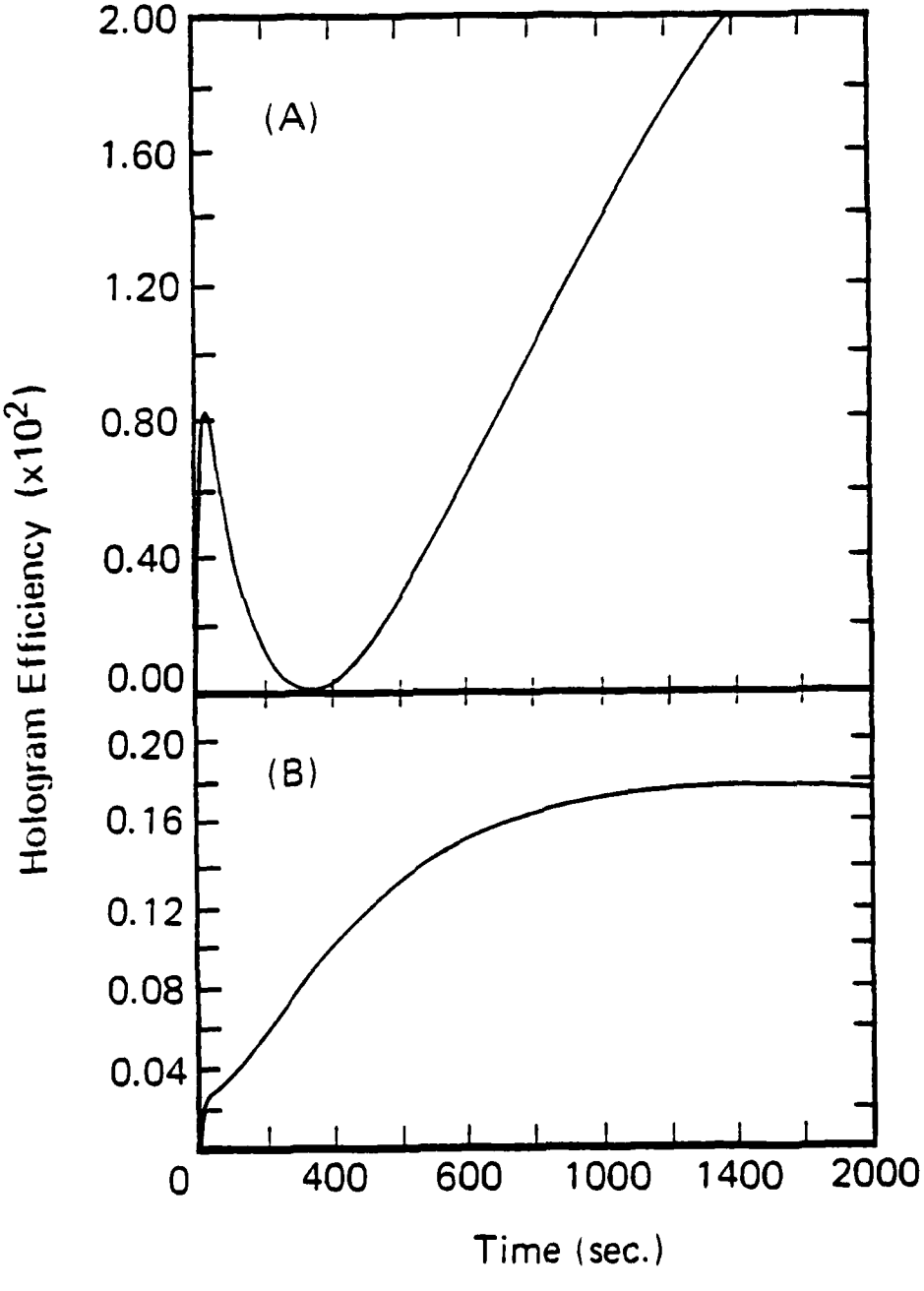

Figure 12. Calculated hologram efficiency vs. time for the consecutive reaction scheme

$$A_1 \xrightarrow{2h\nu} A_2 \xrightarrow{2h\nu} A_3$$

a) Hologram produced and read at 350 nm. b) Hologram produced at 350 nm and read at 514 nm.

SP472-3/A1

472:GAN:716:enj
78u472-608

TECHNICAL REPORT DISTRIBUTION LIST, GEN

	No. Copies
Office of Naval Research Attn: Code 472 800 North Quincy Street Arlington, Virginia 22217	2
ONR Western Regional Office Attn: Dr. R. J. Marcus 1030 East Green Street Pasadena, California 91106	1
ONR Eastern Regional Office Attn: Dr. L. H. Peebles Building 114, Section D 666 Summer Street Boston, Massachusetts 02210	1
Director, Naval Research Laboratory Attn: Code 6100 Washington, D.C. 20390	1
The Assistant Secretary of the Navy (RE&S) Department of the Navy Room 4E736, Pentagon Washington, D.C. 20350	1
Commander, Naval Air Systems Command Attn: Code 310C (H. Rosenwasser) Department of the Navy Washington, D.C. 20360	1
Defense Technical Information Center Building 5, Cameron Station Alexandria, Virginia 22314	12
Dr. Fred Saalfeld Chemistry Division, Code 6100 Naval Research Laboratory Washington, D.C. 20375	1
U.S. Army Research Office Attn: CRD-AA-IP P.O. Box 1211 Research Triangle Park, N.C. 27709	1

	No. Copies
Naval Ocean Systems Center Attn: Mr. Joe McCartney San Diego, California 92152	1
Naval Weapons Center Attn: Dr. A. B. Amster, Chemistry Division China Lake, California 93555	1
Naval Civil Engineering Laboratory Attn: Dr. R. W. Drisko Port Hueneme, California 93401	1
Department of Physics & Chemistry Naval Postgraduate School Monterey, California 93940	1
Scientific Advisor Commandant of the Marine Corps (Code RD-1) Washington, D.C. 20380	1
Naval Ship Research and Development Center Attn: Dr. G. Bosmajian, Applied Chemistry Division Annapolis, Maryland 21401	1
Naval Ocean Systems Center Attn: Dr. S. Yamamoto, Marine Sciences Division San Diego, California 91232	1
Mr. John Boyle Materials Branch Naval Ship Engineering Center Philadelphia, Pennsylvania 19112	1

SP472-3/A1

472:GAN:716:enj
78u472-608

TECHNICAL REPORT DISTRIBUTION LIST, 051A

	No. Copies
Dr. M. A. El-Sayed Department of Chemistry University of California, Los Angeles Los Angeles, California 90024	1
Dr. E. R. Bernstein Department of Chemistry Colorado State University Fort Collins, Colorado 80521	1
Dr. C. A. Heller Naval Weapons Center Code 6059 China Lake, California 93555	1
Dr. J. R. MacDonald Chemistry Division Naval Research Laboratory Code 6110 Washington, D.C. 20375	1
Dr. G. B. Schuster Chemistry Department University of Illinois Urbana, Illinois 61801	1
Dr. A. Adamson Department of Chemistry University of Southern California Los Angeles, California 90007	1
Dr. M. S. Wrighton Department of Chemistry Massachusetts Institute of Technology Cambridge, Massachusetts 02139	1
Dr. M. Rauhut Chemical Research Division American Cyanamid Company Bound Brook, New Jersey 08805	1
Dr. J. I. Zink Department of Chemistry University of California, Los Angeles Los Angeles, California 90024	1
Dr. D. M. Burland K34-281 IBM Corporation 5600 Cottle Road San Jose, CA 95193	1
Dr. John Cooper Code 6130 Naval Research Laboratory Washington, D.C. 20375	1
Dr. William M. Jackson Department of Chemistry Howard University Washington, DC 20059	1
Dr. George E. Walraffen Department of Chemistry Howard University Washington, DC 20059	1

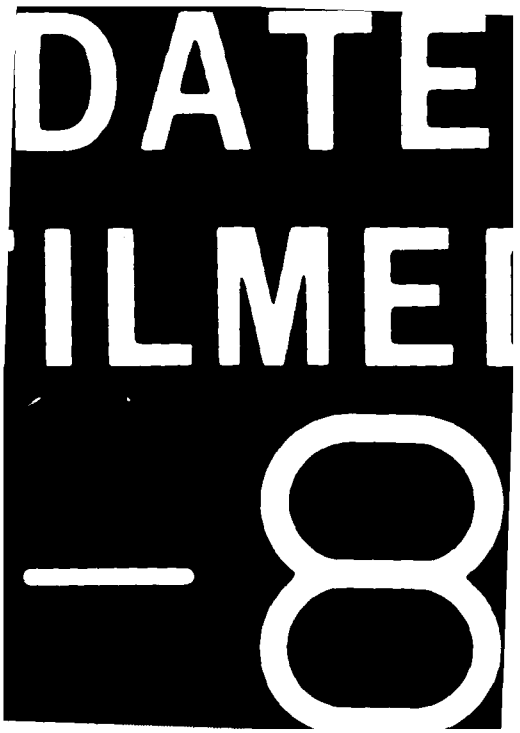
DATE
ILME
8